Relationship between lidar-based observations of aerosol content and monsoon precipitation over a tropical station, Pune, India

P C S Devara, P E Raj, G Pandithurai, K K Dani & R S Maheskumar
Physical Meteorology and Aerology Division, Indian Institute of Tropical Meteorology, Pune 411 008, India

This paper reports the results of the aerosol lidar experiments that have been performed at the Indian Institute of Tropical Meteorology (IITM), Pune (18.54°N, 73.85°E, 559 m amsl), a tropical station in India. The lidar-observed cloud macro-physical parameters (cloud-base and cloud-ceiling heights, vertical thickness, etc.) and polarisation characteristics and their association with surface-generated aerosols at the experimental site are presented and discussed. The correspondence among the lidar-derived aerosol distributions, meteorological parameters and south-west (SW) monsoon (June–September) activity over Pune during 12 successive SW monsoon seasons (1987–98) including two pairs of contrasting seasons of 1987–8 and 1993–4 is also examined. The results indicate an association between variations in aerosol loading in the boundary layer during the pre-monsoon season (March–May) and precipitation intensity during the ensuing monsoon season. Moreover, the decrease in aerosol content from pre-monsoon to monsoon season is found to follow the SW monsoon season total precipitation. Thus the results suggest that (i) the IITM lidar can also be a useful remote sensor for aerosol characterisation studies from polarisation measurements, and some important physical properties of clouds in the lower atmosphere over the station, and (ii) there exists a correspondence between boundary-layer aerosol content and SW monsoon precipitation over Pune, which is explained in terms of the type of aerosols and the environmental and meteorological processes, particularly during pre-monsoon and monsoon months prevailing over the experimental station.

1. Introduction

In recent years, the study of clouds has generated a tremendous amount of research interest because of the complex role of clouds in the earth–atmosphere radiation balance. Atmospheric aerosols play the most crucial role in cloud processes, and observations of aerosol characteristics prior to cloud formation and of the bulk cloud properties after formation would lead to better understanding of the influence of aerosols on clouds. The aerosol–cloud–precipitation cycle is the major mechanism responsible for the modification of aerosols in the troposphere, which leads to cloud growth and subsequent precipitation. Moreover, aerosols and clouds are also important in air pollution as clouds control ventilation of pollutants that are generated at the earth's surface. Their coverage is generally monitored and analysed using satellite data, but sometimes their vertical profile becomes very important. This is difficult to derive from satellite monitoring, but it is relatively easy to achieve by lidar sounding. Moreover, aerosols and clouds are spatially and temporally variable after short periods, so that long-term continuous monitoring with a short repetition time is important.

The amount of solar radiation that reaches the earth's surface depends on the amount of cloud coverage, the type of clouds, and their physical and optical properties. In particular, the optical depth distribution of clouds, which is derivable from the extinction coefficient, is found useful in modelling transport of radiation in the atmosphere (Pal et al. 1992). Therefore, besides the direct radiative effects of aerosols, and thereby the climate, it is important also to consider aerosols as a sub-system of clouds, because of strong interactions between aerosols and clouds (Twomey 1977; Gultepe 1995).

Lidars have been used in the past for cloud studies and have proven adequate in obtaining geometrical cloud parameters (Carswell et al. 1995) and also to retrieve optical cloud parameters (Young 1995). Lidar measurements with excellent spatial and temporal resolution over extended time periods and in different geographical regions provide an instantaneous picture of the

optical properties of clouds. For example, the Experiment Cloud Lidar Pilot Study (ECLIPS) used worldwide lidar observations to gather statistics on cloud-base and cloud-top heights (WMO 1988). The Lidar-In Space Technology Experiment (LITE) program, in which an Nd:YAG lidar was flown on the space shuttle, provided data on vertical profiles of clouds when viewed from above (McCormick et al. 1993). In addition to the multiple scattering technique that is widely used in the optical remote sensing of clouds, polarisation characteristics of lidar return signals provide better description of scattering and composition of clouds such as anisotropy of scatterers as well as water and ice phase determination (Sun & Li, 1989; Sun et al. 1989; Sassen, 1991). Moreover, it is acknowledged that there is a paucity of ground-based lidar observations of clouds over the tropics. Hence, increasing efforts from the international scientific community are being directed towards obtaining ground-based data from tropical sites.

An optical radar or lidar has been operational at the Indian Institute of Tropical Meteorology (IITM), Pune, India since 1985. The main specifications of the lidar system are given in Table 1. The observations are specifically directed to the study of atmospheric aerosol characteristics with a view to establishing climatologies of aerosols, clouds and boundary-layer and air quality parameters, and to investigating their possible connections with concurrent meteorological parameters. In this paper, the results of the lidar-observed cloud macro-physical parameters (cloud base and ceiling heights, vertical thickness, etc.) and their association with surface-generated aerosols and their polarisation characteristics at the experimental site are presented. The observed correspondence between the lidar-derived aerosol content (integration of altitude

profile throughout the height range), meteorological parameters and south-west (SW) monsoon (June–September) activity over Pune during 12 successive SW monsoon seasons (1987–98) including two contrasting seasons of 1987–8 and 1993–4 are discussed.

2. Experimental site characteristics

The lidar site is located at an elevation of about 573 m amsl, approximately 100 km inland from the west coast, and is surrounded by hills as high as 760 m amsl (valley-like configuration). Thus, the transport and dispersion of aerosols, particularly in the lower levels of the atmosphere, are affected by the circulation processes that are produced in this terrain. The major urban activity from the eastern side, and the mixture of water-soluble, dust-like and soot-like aerosols prevailing over the station also influence significantly the aerosol loading at the lidar site. During the pre-monsoon (March–May) very hot weather prevails and cumulonimbus-type cloud development takes place around late afternoon or evening. The airflow in the lower troposphere is predominantly westerly during the SW monsoon season (June–September) which brings in a large influx of moist air from the Arabian Sea. These conditions favour the prevailing aerosol particles in the formation and development of clouds during this season. Thus, almost throughout the season, cloudy sky conditions with occasional breaks of varying duration prevail over the experimental station. The westerly flow weakens in the lower troposphere and the easterly flow sets in during the post-monsoon season (October–November). The continental air mass, rich in nuclei of continental origin, passes over the region during this season. An increase of dry polar continental air in the wake of low pressure systems (western disturbances) takes place during the winter season (December–February). Thus the meteorology at the experimental site varies markedly from continental type (winter) to maritime (summer).

3. Theoretical background

According to the Mie theory, the scattering properties of a sphere of radius r for incident radiation of wavelength λ can be considered in terms of size parameter $x = 2\pi r/\lambda$ and complex index of refraction $m = m_r - m_i$, where m_r and m_i are respectively the refractive and absorptive indices. Scattered intensity in any direction strongly depends on the ratio of particle size to the wavelength of incident radiation. Scattering by particles much smaller than the wavelength is explained by the Rayleigh theory, and particles larger than or comparable to the wavelength by the Mie theory (van de Hulst 1981). At longer wavelengths, scattering due to atmospheric molecules is negligible and the imaginary part of the aerosol refractive index is smaller, hence extinction at these wavelengths is mainly due to scattering.

Table 1: *Main characteristics of the lidar system*

Transmitter	
Laser	Argon ion
Wavelength	0.5145 μm / 0.4880 mm
Output power	4 W (multiline)
Beam divergence	0.283×10^{-6} sr
Beam diameter	1.3 mm
Polarisation	both parallel and perpendicular
Receiver	
Telescope	25-cm φ Newtonian (astronomical quality)
Focal length	190 cm
Collecting area	0.0491 cm²
Divergence	0.5–6.5 m radians
Filter bandwidth	1 nm (FWHM)
Photo-multiplier	RCA C31034A
Photo-multiplier gain	$\geq 10^6$
Cathode efficiency	119 m A / W (typical)
PMT cooler housing	PFR TE-206 TSRF
Pre-amplifier	AD 515J
Transient recorder	Yokogawa multi-pen chart / magnetic tape recorder
Recording format	Signal strength versus altitude

Assuming scattering by poly-disperse spherical particles (aerosols), according to the Mie theory the scattering properties of dielectric spheres for incident radiation of both perpendicular and parallel polarisation can be determined in terms of the size parameter. According to Chylek et al. (1975) and McCartney (1976) the Mie intensity functions for particles having the above characteristics can be written as

$$I_\perp(\theta,x,m)=\left|\sum_{j=1}^{\infty}\frac{2j+1}{j(j+1)}\left[a_j(x,m)\delta_k(\theta)+b_j(x,m)\pi_k(\theta)\right]\right|^2 \quad (1)$$

and

$$I_\parallel(\theta,x,m)=\left|\sum_{j=1}^{\infty}\frac{2j+1}{j(j+1)}\left[a_j(x,m)\pi_k(\theta)+b_j(x,m)\delta_k(\theta)\right]\right|^2 \quad (2)$$

where the quantities a_j and b_j are the Mie coefficients, and $\pi_k(\theta)$ and $\varphi_k(\theta)$ are the angular functions. The Mie scattering function for individual aerosol particles is given as

$$f(\theta,x,m)=[\lambda^2/4\pi^2]I(\theta,x,m) \quad (3)$$

For unit volume of aerosols of different sizes ranging from r_1 to r_2, the scattering cross-section can be written as

$$\sigma_{scat}(\theta)=\int_{r_1}^{r_2}\left(\frac{\lambda^2}{4\pi^2}\right)I(\theta,x,m)n(r)dr \quad (4)$$

Thus the average scattered intensity at any scattering angle θ and for polarised light can also be written as

$$I(\theta)=I_0k^2\cos^2\varphi\int_{r_1}^{r_2}I(\theta,x,m)n(r)dr \quad (5)$$

where $I(\theta)$ is the irradiance of incident light at scattering angle θ; k is wave number (= $2\pi/\lambda$), $n(r)$ is the aerosol number density in the size range from r to $(r+dr)$ and φ is the angle of polarisation of incident light with respect to the scattering plane. The values of r_1 and r_2 considered in the present experiment are 0.1 and 10 μm, respectively.

4. Lidar, observations and analysis

The IITM bi-static Argon-ion lidar system used in the present study has been operational at Pune (18.54°N, 73.85°E, 559 m amsl) since 1985. Table 1 presents the chief characteristics of the lidar system. The complete lidar set-up has been installed on the terrace of the Institute Building so that it is unhindered by tall topographic objects and city light pollution. The detailed description of the experimental set-up can be found in the literature (Devara & Raj 1987; Devara et al. 1995). Collocated with the lidar are multi-channel solar radiometers and a spectroradiometer which also provide column-integrated aerosol optical depth and size distribution during the stable clear-sky

Aerosol lidar experiments and monsoon precipitation conditions (Devara 1998). The observational program includes recording of aerosol vertical profile data on every Wednesday and also on alternate Thursdays in order to coincide with the India Meteorological Department's radiometersonde observations. Apart from these regular measurements, an almost equal number of such profiles have been obtained during various experiments conducted from time to time. Thus more than 620 weekly-spaced vertical profiles of lower atmospheric aerosol number density have been recorded during the 12-year period from October 1986 through September 1998. These profiles form the database for the results presented here.

4.1 Single scattering

In the present experiment, the transmitter and receiver are co-axially separated by a distance of about 60 m in order to operate the lidar in the bi-static mode, since this configuration provides angular distribution of scattered intensity for obtaining aerosol size distribution. The normalised signal strength at different scattering angles (altitudes) has been obtained by operating the lidar system with vertically transmitted laser beam and angular scanning of the receiver in the same plane. At each scattering angle, over 15 observations of both signal and signal plus noise are collected to remove the background noise from the scattering intensity measurements. The difference between the average values of these two datasets will yield the mean signal intensity which is used for computing the received power at each scattering angle. This scattering power is converted into the normalised signal strength (S) by normalising with the power of the laser, the common scattering volume and the path lengths as shown in the following equation. This parameter is used as input data for the retrieval of aerosol number density and cloud macro-physical parameters.

$$S=(P_rR_1^2R_2^2d\omega_1)/(P_TVA_R) \quad (6)$$

where P_R is the received power which can be estimated from the anode current, gain and cathode efficiency of the photo-multiplier; R_1 and R_2 are the ranges from the centre of scattering volume V to the transmitter and receiver, respectively; $d\omega_1$ is the solid angle of the transmitter; P_T is the power of the transmitter; and A_R is the collecting area of the receiver. For bi-static lidar, Eq. (6) becomes

$$S(\theta)=[N\sigma_{scat}(\theta)]T(\theta)\eta \quad (7)$$

where N is aerosol number density, $\sigma_{scat}(\theta)$ and $T(\theta)$ are differential Mie scattering cross-section and atmospheric transmittance along the transmitter-receiver path at scattering angle θ, η is the system constant including overall optical efficiencies of the transmitter and receiver.

Combining eqs. 4 and 7, we get

$$S(\theta) = N\eta T(\theta)\left[\int_{r_2}^{r_1}\left(\frac{\lambda^2}{4\pi^2}\right)I(\theta,x,m)n(r)dr\right] \tag{8}$$

Since the scattering in the atmosphere is caused by aerosols as well as molecules, Eq. (6) can be written as

$$S(\theta) = [Na\sigma_a(\theta) + N_m\sigma_m(\theta)]T(\theta)\eta \tag{9}$$

where N_a and N_m are concentrations, $\sigma_a(\theta)$ and $\sigma_m(\theta)$ are differential Mie scattering cross-section at scattering angle θ for aerosols and molecules respectively. In order to apply the inversion method, which is described below, to the scattered intensity recorded at different scattering angles, we assume that aerosol consists of homogeneous spherical particles with radius r and complex index of refraction m (i.e., particle composition) with its imaginary component negligible at visible wavelengths (Shettle & Fenn 1979). These assumptions are necessary to permit tractable calculations of the light scattering properties of poly-disperse collections of randomly oriented, irregularly shaped particles of varying composition.

On obtaining the normalised signal strength values at each scattering angle, they are inverted by following the method described in our earlier publications (Devara & Raj 1989; Devara et al. 1995). The size distribution was assumed to follow a modified power law distribution as suggested by McClatchey et al. (1972), which is given by

$n(r) = C\,10^v$ (for r values between 0.02 μm and 0.1 μm)

$n(r) = C\,r^v$ (for r values between 0.1 μm and 10 μm)

$n(r) = 0$ (for all other values of r) \qquad (10)

where $n(r)$ is the number of particles with radii between r and $(r + dr)$ in unit volume, v is the size index and C is the normalisation constant that follows from the continuity.

$$n(r)dr = n_{total}\,(\text{cm}^{-3}) \tag{11}$$

The lidar was operated at its wavelength of 0.5145 μm and with a separation of about 60 m between the transmitter and receiver to obtain observations of laser-return signal intensity at different scattering angles. The aerosol number density profile obtained after each lidar experiment has been integrated up to an altitude of 1100 m to compute aerosol columnar content in the atmospheric boundary layer over the experimental station using the following expression.

$$\sum_{i=50}^{1100}\left(\frac{C_i + C_{i+1}}{2}\right)(h_{i+1} - h_i)\quad cm^{-2} \tag{12}$$

where C_i and C_{i+1} are concentration at heights h_i and h_{i+1} respectively. The surface and altitude profile data of meteorological parameters at the experimental sta-

tion during the 12-year period of lidar observations have also been collected from the India Meteorological Department, which is almost 3 km east of the lidar site.

4.2 Multiple scattering

As long as the sky is clear, the laser return signal strength can be considered to be due to single scattering phenomenon as explained above, but when laser light propagates through a dense (or turbid) atmosphere with haze, fog or clouds, it undergoes multiple scattering before it is measured by the receiver of the lidar system as demonstrated in Figure 1. It is evident that when the beam enters the cloudy atmosphere it broadens owing to forward scattering of the cloud droplets and the resultant increase in optical cross-section, and the return signal will have a contribution from the multiple scattering process. The areas marked A, B and C in Figure 1 refer to the illuminated area which results from pure multiple scattering in the absence of any single scattering contribution. This is normally measured by fitting the lidar receiver with a focal plane stop so that area A cannot be viewed by the system. In other words, in multiple scattering, some of the light energy which for single scattering would be lost from the transmitted beam is scattered back into the beam and reduces the effective extinction coefficient of the medium. Thus, multiple scattering leads to a higher transmittance of the laser beam compared to the case where only single scattering is considered (Gordon 1982). Such information obtained with the lidar set-up on two typical days (23 June 1997 and 22 June 1998) associated with cloudy sky is depicted in Figure 2. The presence of double cloud layers is evident on both days. The basic cloud physical parameters, such as cloud base (B.H) and ceiling (C.H) heights, are indicated in the figure for each observational day.
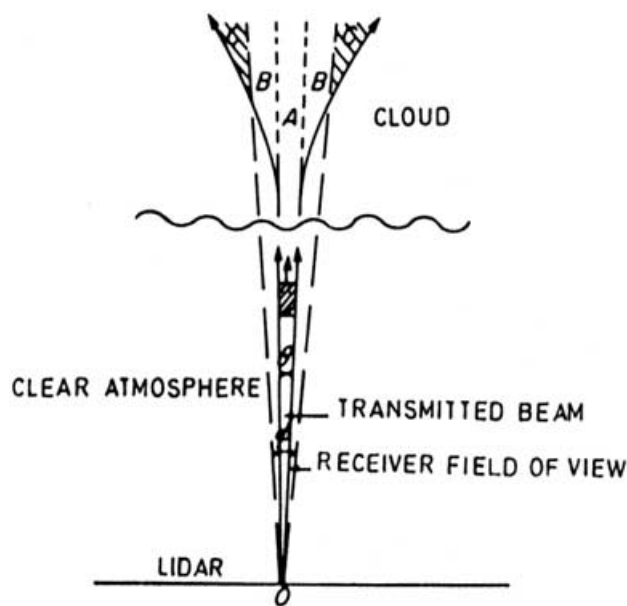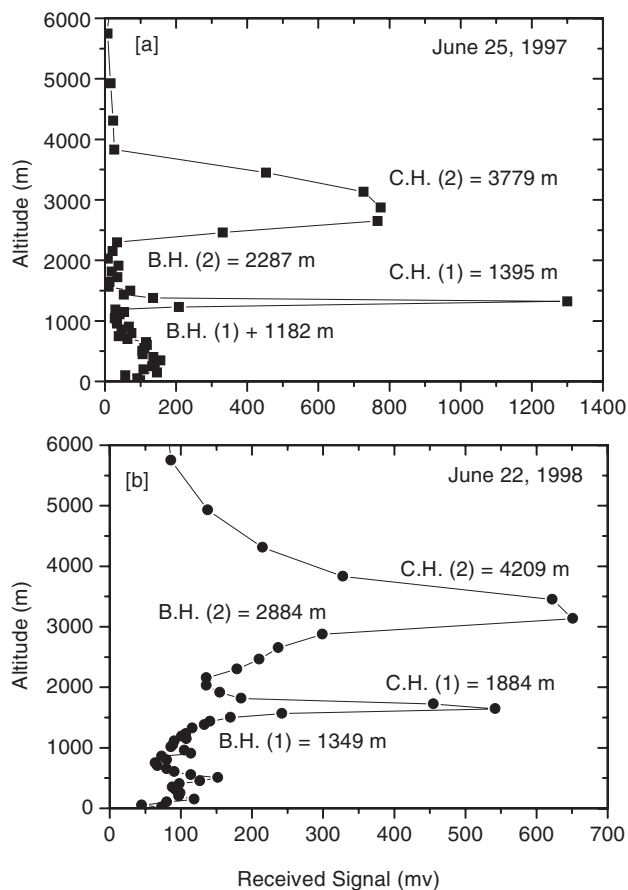

Figure 1. *Schematic representation of lidar behaviour in a turbid medium (after Carswell 1983).*

5. Polarisation characteristics of aerosol scattering

In general, the scattered radiation from atmospheric aerosols is elliptically polarised. Even when the incident light wave is plane polarised with the plane of polarisation parallel or perpendicular to the scattering plane, scattered radiation will contain both parallel and perpendicular polarised components. This is mainly because of anisotropy of aerosol scattering. If the aerosols are assumed to be isotropic, the polarisation component along the principal directions are equal and the components in all other directions vanish. This implies that for isotropic polarisability, if the incident wave is plane polarised with the plane of polarisation parallel to the scattering plane, the scattered radiation contains only the parallel component, and if the incident wave is plane polarised with the plane of polarisation perpendicular to the scattering plane, the scattered radiation contains only the perpendicular component. This means that no depolarisation occurs. Thus the amount of depolarisation is a measure of the anisotropy of the scatterer. The degree of polarisation gives the relative contribution of each polarisation component to the isotropy or anisotropy behaviour of the scatterer. Thus the scattering properties of atmospheric aerosols differ significantly with the state of polarisation of incident laser radiation.

As explained above, for an incident non-polarised light, the parallel and perpendicular polarisation components will be affected unequally by the scattering phenomenon. This amounts to some polarisation effect for the incident non-polarised light. By making lidar measurements of aerosols with both parallel and perpendicular polarised laser light, it is possible to study the parameters such as degree of polarisation and depolarisation ratio. These parameters will be very useful for studying the isotropy/anisotropy of scattering characteristics of atmospheric aerosols during different weather conditions. These parameters will also provide information on the micro-physics of raining and/or non-raining clouds. The results of the polarisation lidar measurements obtained on the typical days (14 May and 7 August 1997) are shown in Figures 3 and 4. Each of these figures shows the normalised signal strength profiles obtained with the incident parallel and perpendicular polarised Argon ion laser light at a wavelength of 0.5145 μm. The corresponding profiles of degree of polarisation (P) and depolarisation ratio (D), both in per cent, are computed using the following equations

$$P = [(I_{\perp} - I_{||}) / (I_{\perp} + I_{||})] \times 100 \qquad (13)$$

$$D = I_{\perp} / I_{||} \qquad (14)$$

where $I_{\perp}$ and $I_{||}$ are the normalised signal strengths recorded by the lidar at its perpendicular and parallel polarisation, respectively. It may be noted here that the profiles on 14 May were obtained up to about 3 km
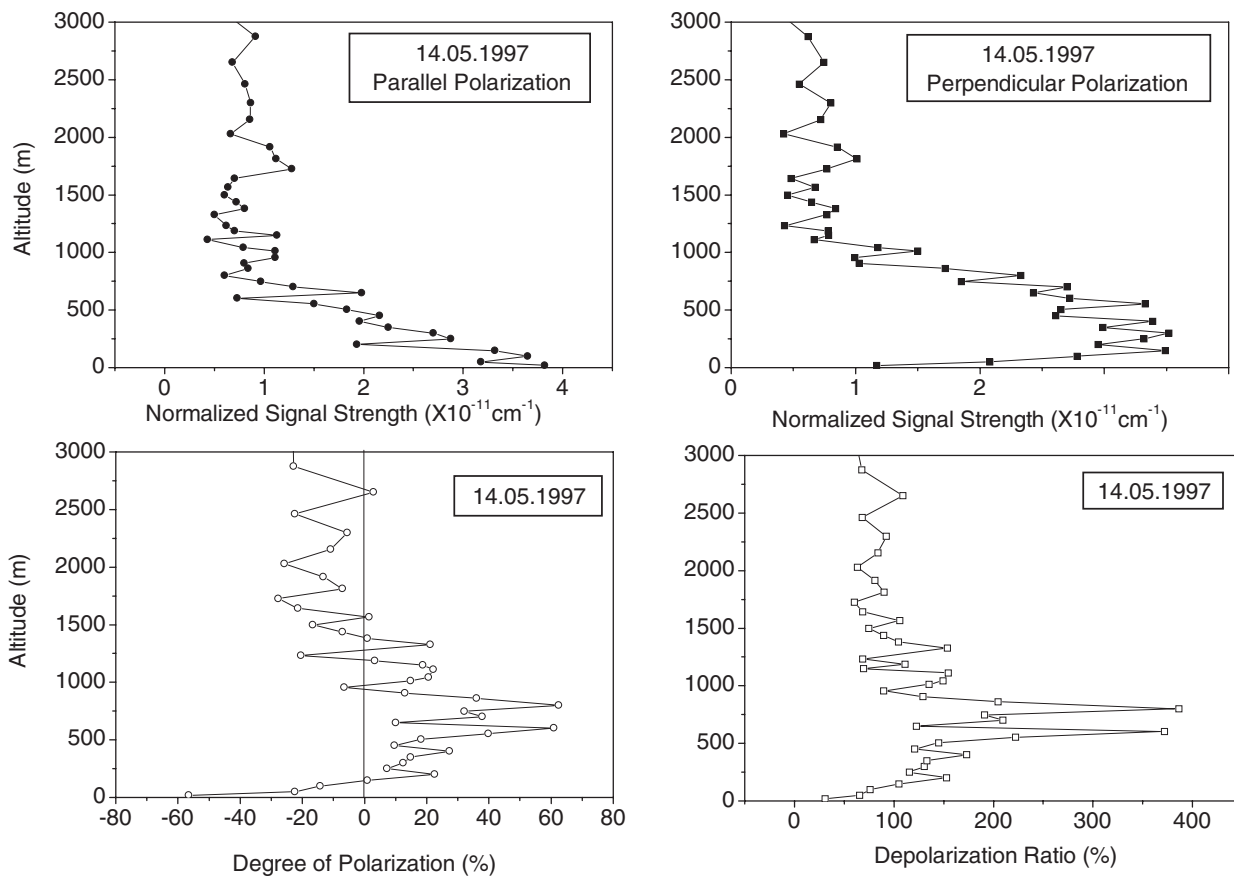

Figure 2. *Typical profiles of lidar-measured scattered signal strength on (a) 25 June 25 1997 and (b) 22 June 1998. The profiles clearly depict multiple cloud layer structures. The heights of the cloud-base (B.H.) and cloud-ceiling (C.H.) observed on both days are also indicated.*

The multiple scattering coefficient depends on the field-of-view (FOV) of the laser transmitter and receiver. It also depends on the distance of the receiver to the scattering medium, its optical properties and density (Gordon 1982; Spinhirne 1982). The influence of multiple scattering on the propagation of the lidar signal can be calculated by using analytical methods (Liou 1971). Measuring the polarisation components of the scattered layer with a lidar system allows the estimation of higher orders of scattering. Using different field stop apertures (Allen & Platt 1977) makes it possible to distinguish between FOVs where single scattering is dominant and FOVS where multiple scattering is dominant. Measuring polarisation at different FOVs thus makes it possible to determine the multiple to single scattering ratio. The results of the analytical and statistical methods indicate that multiple scattering has to be considered not only when analysing the lidar signals from dense media such as fog and water clouds (Platt et al. 1989) but even from a cloudless sky. Atmosphere multiple scattering cannot be neglected when measuring particles from long distances such as from a space lidar with a FOV of more than 1 milliradian (Spinhirne 1982). Multiple scattering effects cannot be neglected in the lidar scattering even from episodes of dense air pollution, dust storms and volcanic eruptions.

Figure 3. *Characteristics of scattered signal strength profiles recorded with parallel and perpendicular polarised laser light on a typical experimental day during May 1997.*
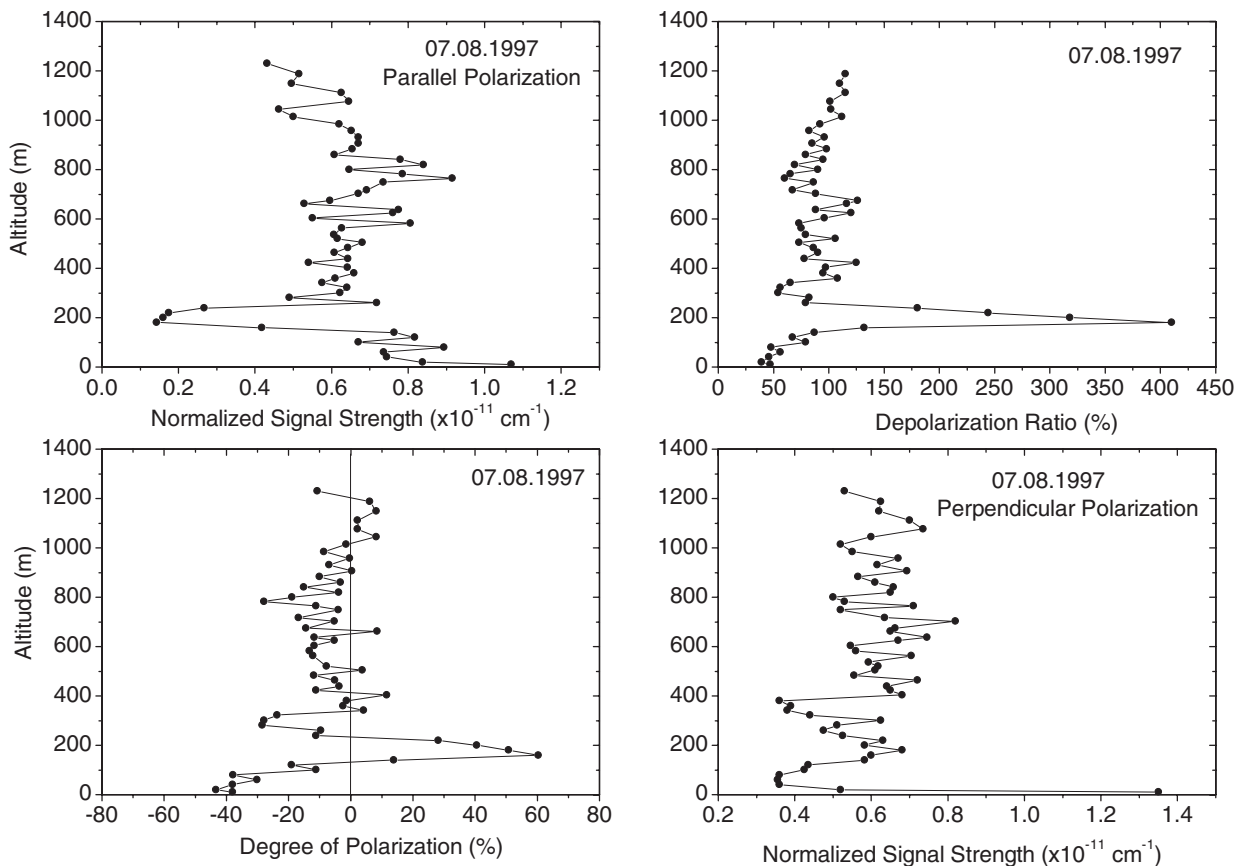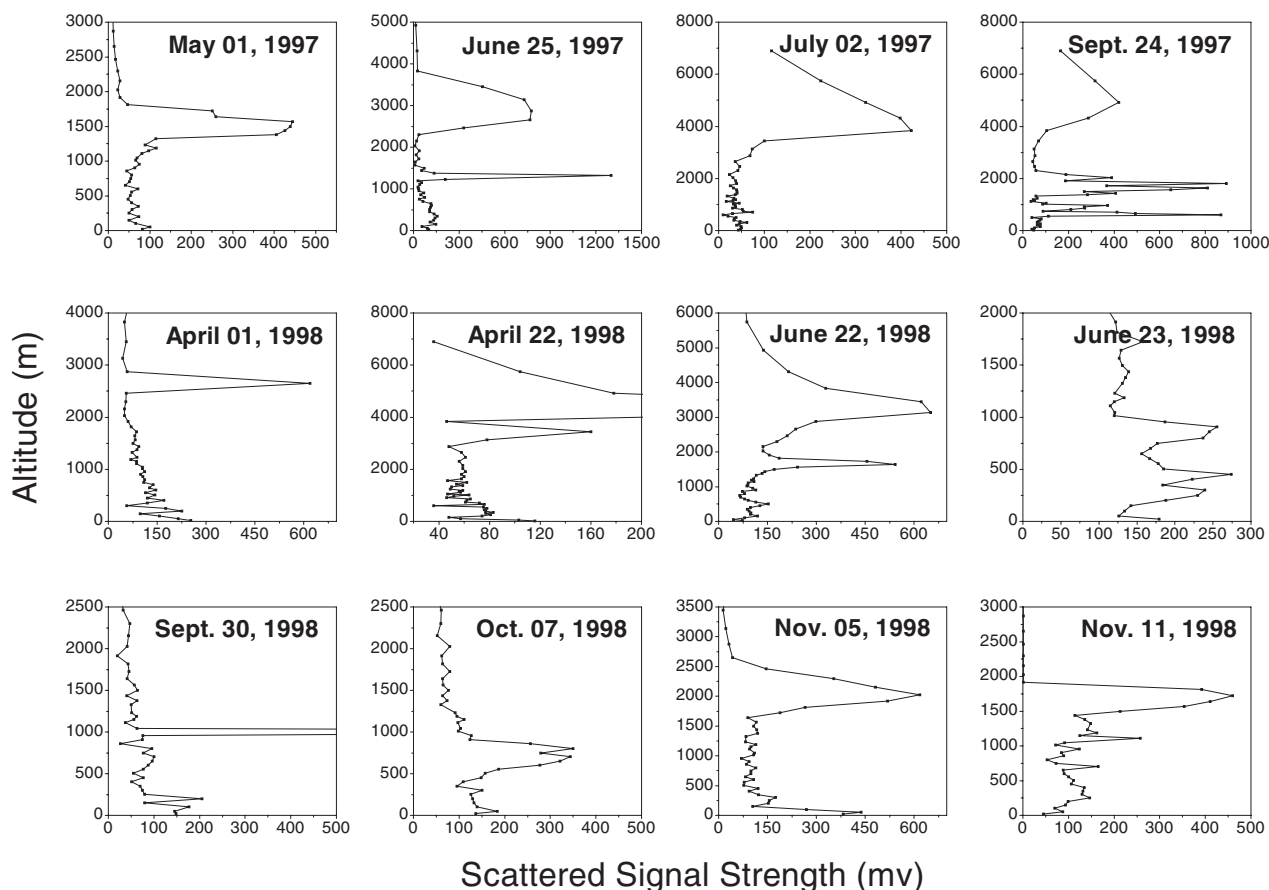

Figure 4. *As for Figure 3 but observed within the boundary layer on 7 August 1997.*

Figure 5. *Set of lidar scattered signal strength profiles and the retrieved cloud macrophysical parameters on some selected cloudy days during 1997 and 1998. The profiles shown in Figure 2 are also included in the set to demonstrate clouds of different layer structures, particularly in the sub-cloud region.*

whereas the profiles on 7 August were obtained up to about the boundary layer altitude. The per cent degree of polarisation yields the relative share of each component of the integrated effect of incident polarisation on the scatterers. The positive values of per cent degree of polarisation represent more contribution from perpendicular component while the negative values suggest the dominance of parallel component to the scattered signal.

The vertical distribution of depolarisation ratio exhibits significant variation with altitude. On both the observational days, the variations are large in the boundary layer, which indicate that the aerosol particles in this region are more isotropic. It is also evident that this anisotropic behaviour decreases with increase in altitude, being more prominent in the regions of aerosol layer formation. Thus the results of the present study imply that particles in the sensing region are not completely spherical in shape. Decrease of depolarisation ratio with altitude occurs mainly due to reduction in particle concentration with height which is also consistent with the observation of larger ratios in the region of aerosol layer formation due to atmospheric stability. Thus, the present results reveal that the aerosol particles in the lower altitudes over the experimental station are more anisotropic. It is planned in the future work to utilise such polarisation measurements under cloudy-sky conditions for studying the properties of raining and/or non-raining clouds over the experimental station.

6. Aerosol-cloud relationship

The study of clouds is one of the important applications of lidar to meteorology. Aerosols of giant size (radius > 1 μm) act as cloud condensation nuclei (CCN) or ice nuclei (IN), and they play a pivotal role in the formation of clouds and their time evolution (Twomey 1977). Owing to a high density of nuclei with large optical cross-sections in clouds, lidar can be used to study clouds and their micro-physics (Zuev 1982). In the presence of clouds, the received laser-scattered signal strength increases enormously, sometimes by several orders of magnitude. This is mainly due to multiple scattering. Though the multiple scattering component also contributes to the total lidar return signal strength, its contribution is far smaller than that of the multiple scattering component. Thus lidar is also a very useful tool for determining cloud macrophysical parameters. This phenomenon of multiple scattering in clouds, and the recently developed UV lidar techniques, have been receiving much attention in recent years in the development of space lidar (Winker et al. 2002; Roy et al. 2002; Flamant 2002).

Figure 5 demonstrates the ability of the lidar used in the present study to determine cloud physical parameters such as base, ceiling heights and vertical thickness from the lidar signal strength profile observations obtained on some typical days during the pre-, during and post-monsoon months. The multiple cloud layers and different fine-scale atmospheric structures below the first cloud base from the ground, as well as between the cloud layers, can be clearly seen. Interaction between the surface-generated aerosols and the structure of low and medium clouds can be an important effect over urban environments (Oke 1987; Collier 2002). Furthermore, the fine structure of scattering in the air layer below the clouds can yield useful information on the properties of clouds forming over different geographical regions. Some of these aspects have been studied by comparing the lidar-measured aerosol number density distributions on consecutive clear-sky and cloudy-sky days to explain the underlying mechanism of 'cloud scavenging' over the experimental station (Devara et al. 1998).

7. Aerosol-precipitation relationship

Most parts of India receive rainfall during the SW monsoon season. The relationship between boundary-layer

aerosols and precipitation over the Pune region over the 12 successive SW monsoon seasons, covering two contrasting monsoons, have been examined utilising the coincident, multi-year lidar aerosol and precipitation data for the period from 1987 to 1998. The aerosol columnar content or loading during different months of 1987 and 1993 (weak monsoon years) and 1988 and 1994 (active monsoon years) are depicted in Figures 6 and 7 respectively. Since aerosols present in the air layers close to the ground contribute significantly to the total loading, the mean content in the air layer between 50 m and 200 m during different months are also shown in the figures. The total rainfall during the 1987 SW monsoon season was 380 mm while during 1988 it was 885 mm. The mean aerosol content during the pre-monsoon season (March-May) in 1987 was 129×10^6 cm^{-2} while during 1988 it was 179×10^6 cm^{-2}. The total rainfall during the SW monsoon season in 1993 was 428 mm while in 1994 it was 774 mm. The mean aerosol content during the pre-monsoon of 1993 was 168×10^6 cm^{-2} compared with 177×10^6 cm^{-2} in 1994. Thus the results suggest a correspondence between the SW monsoon activity and pre-monsoon aerosol loading over Pune.

The above aerosol-precipitation relationship has also been further explored using long-term data collected during the 12-year period. The decrease in aerosol columnar content from pre-monsoon (convection) to monsoon (rain washout) seasons is found to be about
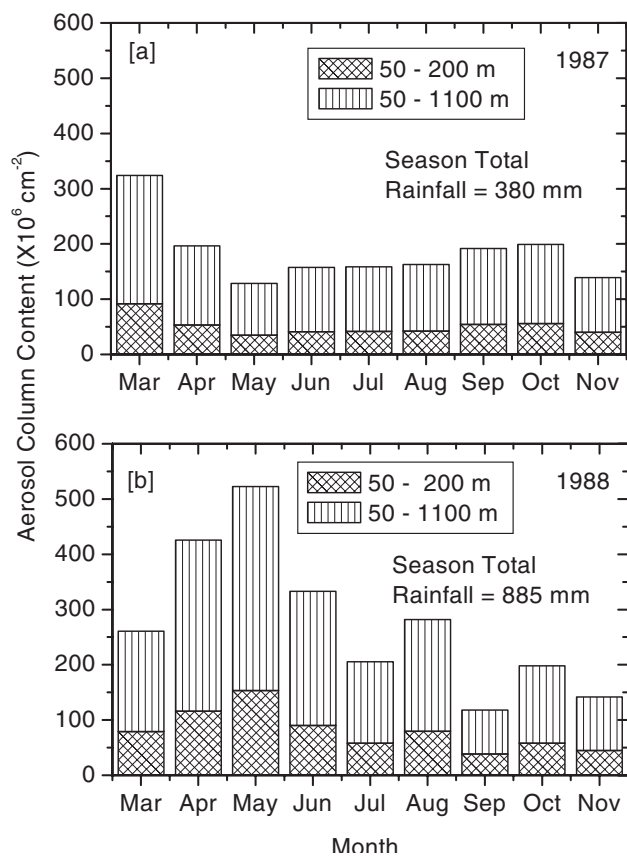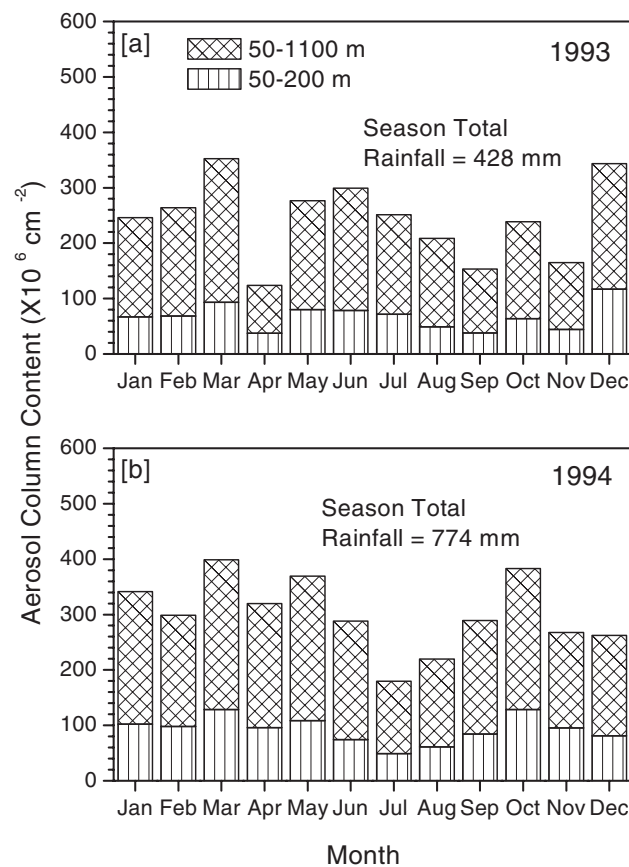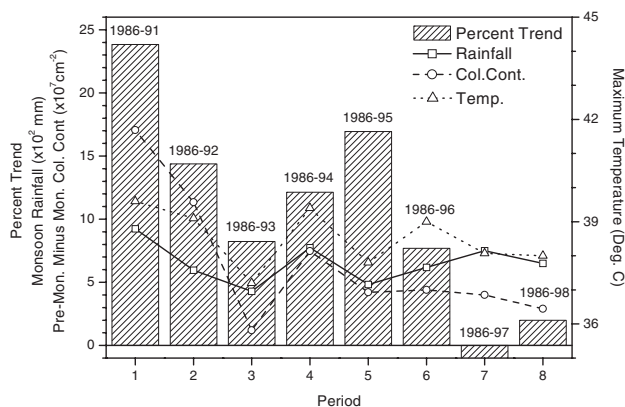

Figure 6. Lidar-derived monthly mean aerosol columnar content in the boundary layer during two contrasting south-west monsoon years of 1987 and 1988. Note the contributions to the aerosol content from the air layer at 50–200 m (layer close to ground and more representative of anthropogenic activities around the site) compared with the 50–1100 m layer.

Figure 7. As for Figure 6 but for another pair of contrasting monsoon years, 1993 and 1994.

260

Figure 8. *Correspondence between aerosol columnar content, monsoon precipitation and temperature during 12 successive SW monsoon seasons. The average of five years' data (1986–1991) is considered as the initial database, which is updated subsequently with the data collected during every year.*

40 per cent and shows a close association with the monsoon season total rainfall. This interesting feature is demonstrated (Figure 8) by comparing the year-to-year change in aerosol loading (trend in per cent) and pre-monsoon minus monsoon aerosol columnar content, SW monsoon season total rainfall and the maximum temperature that occurs during March every year over the experimental station. In the computation of year-to-year percentage change in the aerosol loading, the cumulative trend observed in the data for the first five years is considered as the initial long-term database and is updated every year by adding the lidar-derived aerosol columnar content data for that year. It is evident from Figure 8 that all four parameters exhibit co-variation up to 1994, which is possible because an increase in columnar content results in an increasing trend and aerosol rainfall over this station. In addition, the negative correlation exhibited by the percentage trend during 1995 and 1996 is considered to be due to non-uniform distribution of precipitation during those years.

The experimental station received rainfall of 618, 741 and 649 mm during SW monsoon seasons of 1996, 1997 and 1998 respectively. In 1997, the annual total precipitation intensity was greater (1027 mm) than that during 1996 (820 mm) and 1998 (813 mm). Since the precipitation was distributed over the whole year, in 1997 the washout and rainout mechanisms might have acted more effectively on the aerosol loading over the station and altered the trend from positive to negative.

The above correspondence between the aerosol columnar content and SW monsoon precipitation over Pune could be due to the combined effect of the type of local aerosols and associated radiative forcing induced by dynamics and the transport of marine air masses from the Arabian Sea during the SW monsoon season. This feature suggests that a change in pre-monsoon aerosol loading has a bearing on the ensuing SW monsoon pre-

Aerosol lidar experiments and monsoon precipitation

cipitation. Such a relationship would be valuable in inferring the behaviour of monsoons from long-term aerosol observations.

References

Allen, R. J. & Platt, C. M. R. (1977) Lidar for multiple backscattering and depolarization observations. *Appl. Opt.* **16:** 3193–3199.

Carswell, A. I. (1983) Lidar measurements of the atmosphere. *Can. J. Phys.* **61:** 378–395.

Carswell, A. I., Fong, A., Pal, S. R. & Pribluda, I. (1995) Lidar-derived distribution of cloud vertical location and extent. *J. Appl. Meteor.* **34:** 107–120.

Collier, C. G. (2002) Developments in radar and remote-sensing methods for measuring and forecasting rainfall. *Phil. Trans. Royal Soc. of London Series A* **360:** 1345–1361.

Chylek, P., Grams, G. W., Smith, G. A. & Russell, P. B. (1975) Hemispherical backscattering by aerosols. *J. Appl. Meteorol.* **14:** 380–387.

Devara, P. C. S. (1998) Remote sensing of atmospheric aerosols from active and passive optical techniques. *Int. J. Remote Sensing* **19:** 3271–3288.

Devara, P. C. S. & Raj, P. E. (1987) A bistatic lidar for aerosol studies. *J. Inst. Electron. Telecommun. Eng. Tech. Rev.* **4:** 412–415.

Devara, P. C. S. & Raj, P. E. (1989) Remote sounding of aerosols in the lower atmosphere using a bistatic CW Helium-Neon lidar. *J. Aerosol Sci.* **20:** 37–44.

Devara, P. C. S., Raj, P. E., Sharma, S. & Pandithurai, G. (1995) Real-time monitoring of atmospheric aerosols using a computer-controlled lidar. *Atmos. Environ.* **29:** 2205–2215.

Devara, P. C. S., Pandithurai, G., Raj, P. E., Maheskumar, R. S. & Dani, K. K. (1998) Atmospheric aerosol-cloud-stability relationship as observed with optical and radio remote sensing techniques. *Atmos. Res.* **49:** 65–76.

Flamant, P. H. (2002). ESA <<EOLUS-ADM>> to probe atmospheric winds from space. In: *Lidar Remote Sensing in Atmospheric and Earth Sciences*, L.R. Bissonnett, G. Roy & G. Vallee (eds.), Defence R&D Canada, Valcartier, Canada, pp. 815–816.

Gordon, H. R. (1982) Interpretation of airborne oceanic lidar: effects of multiple scattering. *Appl. Opt.* **21:** 2996–3001.

Gultepe, I., 1995. Physical, radiative and dynamical processes within a nighttime marine stratus cloud. *PAGEOPH* **144:** 321–350.

Liou, K. (1971) Time dependent multiple backscattering and depolarization from water clouds for a pulsed lidar system. *J. Atmos. Sci.* **28,** 772–784.

McCartney, E. J. (1976) *Optics of the Atmosphere: Scattering by Molecules and Particles*. Wiley: New York.

261

McClatchey, R. A., Fenn, R. W., Selby, J. E. A., Volz, F. E. & Garing, J. S. (1972) *Optical Properties of the Atmosphere*. AFCRL–72–0497, Air Force Cambridge Research Laboratories, Bedford.

McCormick, M. P., Winker, D. M., Browell, E. V., Coakley, J. A., Gardner, C. M., Hoff, R. M., Kent, G. S., Melfi, S. H., Menzies, R. T., Platt, C. M. R., Randall, D. A. & Reagan, J. A. (1993) Scientific investigations planned for the Lidar In-Space Technology Experiment (LITE). *Bull. Am. Meteorol. Soc.* **74**: 205–214.

Oke, T. R. (1987). *Boundary Layer Climates*, 2nd edn, Methuen: London.

Pal, S. R., Steiinbrecht, R. W. & Carswell, A. I. (1992) Automated method for lidar determination of cloud-base height and vertical extent. *Appl. Opt.* **31**: 1488–1494.

Platt, C. M. R., Spinhirne, J. D. & Hart, W. D. (1989) Optical and microphysical properties of cold cirrus cloud: evidence for regions of small ice particles. *J. Geophys. Res.* **94**: 11.151–11.164.

Roy, G., Bissonnette, L. R. & Poutier, L. (2002) Space based MFOV lidar and ABL aerosols. In: *Lidar Remote Sensing in Atmospheric and Earth Sciences*, L.R. Bissonnett, G. Roy & G. Vallee (eds.), [add publisher + place of publishing] pp. 747–750.

Sassan, K. (1991) The polarization lidar technique for cloud research : A review and current assessment. *Bull. Amer. Meteorol. Soc.* **72**: 1848–1866.

Shettle, E. P. & Fenn, R. W. (1979) *Models for the Aerosols of the Lower Atmosphere and the Effects of Humidity Variations on their Optical Properties*, AFGL-TR-79–0214, Air Force Geophysics Laboratory, Hanscom AFB, MA.

Spinhirne, J. D. (1982). Lidar clear atmosphere dependence on receiver range. *Appl. Opt.* **21:** 2468–2476.

Sun, Y.-Y. & Li, Z.-P. (1989) Depolarization of polarized light caused by high altitude clouds. Part 2: Depolarization of lidar induced by water clouds. *Appl. Opt.* **28:** 3633–3638.

Sun, Y.-Y., Li, Z.-P. & Bosenberg, J. (1989) Depolarization of polarized light caused by high altitude clouds. Part 1: Depolarization of lidar induced by cirrus clouds. *Appl. Opt.* **28:** 3625–3632.

Twomey, S. (1977) *Atmospheric Aerosols*. Elsevier: New York, 302 pp.

van de Hulst, H. C. (1981) *Light Scattering by Small Particles*. Dover: New York.

Winker, D. M., Pelon, J. & McCormick, M. P. (2002) The CALIPSO Mission : Aerosol and cloud observations from space. In: *Lidar Remote Sensing in Atmospheric and Earth Sciences* L. R. Bissonnette, G. Roy & G. Vallee (eds.), Defence R&D Canada, Valcartier, Canada, pp. 735–738.

World Meteorological Organization (WMO) (1988) Cloud-base Measurement Workshop. Report of the WCRP/CSIRO.

Young, S. A. (1995) Analysis of lidar backscatter profiles in optically thin clouds. *Appl. Opt.* **34:** 7019–7031.

Zuev, V. E. (1982) *Laser Beams in the Atmosphere*, Plenum: New York, 504 pp.